Probing the Nature of Surface Barriers on ZSM-5 by Surface Modification

Guanghua Ye[1,‡], Zhongyuan Guo[1,‡], Yuanyuan Sun[1], Kake Zhu[1], Honglai Liu[1], Xinggui Zhou[1,*], and Marc-Olivier Coppens[2,*]

DOI: 10.1002/cite.201700081

Supporting Information available online

Dedicated to Prof. Dr. Frerich J. Keil on the occasion of his 70th birthday

The nature of external surface barriers in the zeolite ZSM-5 was explored by comparing mass transfer of *n*-heptane in samples with different crystal sizes, surface structure, and composition. These different surface properties were achieved by HF acid etching and SiO_2 deposition on an as-synthesized ZSM-5 crystal sample. HF etching does not reduce surface barriers. SiO_2 deposition on the same sample reduces surface barriers significantly. These insights into the nature of surface barriers could be used to guide the rational design of zeolitic materials with better mass transport properties.

Keywords: HF etching, *n*-Heptane, SiO_2 deposition, Surface barriers, ZSM-5

Received: July 11, 2017; *revised:* August 06, 2017; *accepted:* August 07, 2017

1 Introduction

Zeolites are crystalline aluminosilicates with well-defined micropore networks and tunable active sites. Thus, they have found numerous important applications in the areas of separation and catalysis. The molecular-sized micropores ($d_{pore} < 2$ nm) endow zeolites with the great advantage of shape selectivity [1], on the one hand, but severely limit diffusion of molecules in zeolites [2], on the other hand. To reduce intracrystalline diffusion limitations, a straightforward approach is to shorten the diffusion path length to the nanoscale, which has stimulated great interest in synthesizing hierarchical zeolites [2 – 5]. However, some recent studies using zero length column (ZLC) [6 – 8] and frequency response (FR) [9] methods have found that the apparent diffusivities for nano-sized zeolites can be several orders of magnitude lower than the ones for micro-sized zeolites. Such studies [6 – 9] suggest that, besides intracrystalline diffusion resistance, surface transport resistances known as surface barriers also exist and can even play a dominant role in determining the rate of mass transport, especially for nano-sized zeolites. Meanwhile, in catalysis, Rao et al. [10] evidenced the important role of surface barriers in affecting the activity of ZSM-5 for catalyzing alkylation of benzene with ethylene. To rationally design zeolitic materials for catalysis and separation, it is essential to understand the exact nature of surface barriers.

Transport across the surface and intracrystalline diffusion together constitute the overall mass transfer of molecules from the gas phase into a zeolite crystal, or the other way around. The surface transport can be further divided into a series of elementary steps (including molecules adsorbing on the external surface of zeolites and entering into or leaving surface pores) on the surface layer that separates the gas-phase region from the core zeolite space, as revealed by Lercher et al. [11, 12] using time-resolved rapid-scan IR spectroscopy. Thus, the surface barriers should be tightly linked to the properties of this surface layer.

[1]Dr. Guanghua Ye, Zhongyuan Guo, Yuanyuan Sun, Prof. Kake Zhu, Prof. Honglai Liu, Prof. Xinggui Zhou
xgzhou@ecust.edu.cn
East China University of Science and Technology, State Key Laboratory of Chemical Engineering, 130 Meilong Road, Shanghai 200237, China.

[2]Prof. Marc-Olivier Coppens
m.coppens@ucl.ac.uk
University College London, Department of Chemical Engineering, Torrington Place, London WC1E 7JE, UK.

[‡]Both authors contributed equally to this paper

Pore blockage on the external surface of zeolites is believed to be one important origin of surface barriers. For silicalite-1 with MFI structure, Dauenhauer et al. [7, 8, 13] attributed its surface barriers primarily to the blockage of surface pores and estimated that over 99.9 % of its surface pores could be blocked, using ZLC and FR experiments, as well as molecular simulations. For Zn(tbip), a nanoporous metal-organic framework (MOF), Kärger et al. [14, 15] reached a similar conclusion that the surface barriers on this material arise from the complete blockage of surface pores, using microscopic diffusion measurements and mesoscopic modeling. The exact nature of surface pore blockage is still uncertain. Mechanistically, the surface pore blockage could originate from the presence of an amorphous phase or uncoordinated lattice on the external surface, which has interpenetrating dangling silanol bonds [16, 17]. Besides, the surface pore blockage could also arise from structural imperfections, including bridging across pores, surface pore narrowing, and pore misalignment, although existing experimental techniques are still unable to directly observe these imperfections [8, 13].

Differences in the atomistic force fields experienced by molecules in the gas phase and the adsorbed phase can be another reason for the surface barriers on zeolites. Keil et al. [18 – 21] studied the diffusion of molecules in several zeolites (AFI, LTL, LTA, and MFI) by performing extensive molecular simulations, and they evidenced the presence of surface barriers even without steric surface pore blockage. They attributed these surface barriers to the large free energy differences between gas phase, zeolite surface, and zeolite interior. Similar or related explanations on surface barriers were also given in other literature [22 – 27]. During an uptake process, the entropic barrier could also be a source of surface barriers, since molecular rearrangement is required before entering into surface pores and this rearrangement could reduce the pre-exponential for diffusion [11, 28].

Hence, although extensive experiments and simulations were carried out in an attempt to understand the nature of surface barriers on zeolites, the exact causes for these surface barriers remain unclear. Generally, the surface properties of zeolites determine surface barriers. However, it seems almost impossible to precisely determine the surface properties of zeolites by using the existing imaging techniques, because of their limitation in resolution (~5 Å) [29, 30], therefore, it is very difficult to directly correlate surface barriers with surface properties. Surface modification techniques, such as chemical etching and chemical liquid deposition (CLD), can change the surface properties of zeolites. For example, HF acid etching can remove the surface layer in which large amounts of amorphous phase and structural imperfections are located, as HF reacts with both silicon and aluminum [16, 31]. Chemical liquid deposition of tetraethyl orthosilicate (TEOS) can deposit a layer of amorphous SiO_2 over the surface layer. This amorphous SiO_2 may block or narrow surface pores and increase the rigidity of these pores, on the one hand, but may also enhance surface adsorption and increase sticking coefficients of molecules, on the other hand [28]. Therefore, combining surface modification and macro/microscopic techniques of diffusion measurements [32, 33] could provide a new opportunity to indirectly probe the nature of surface barriers on zeolites.

Some efforts have been made to investigate the effects of surface modification on mass transfer in zeolites, but seemingly contradictory results were obtained. Wloch [34] found that the adsorption of hexane on ZSM-5 was accelerated after zeolite crystals were purified through HF etching, and similar findings were also reported for other sorption systems [16, 35]. Chmelik et al. [36] and Gueudré et al. [37], however, reported that HF etching of silicalite-1 crystals did not change the sorption rates of isobutene and cyclohexane, respectively. Lercher et al. [28, 38, 39] deposited a layer of amorphous SiO_2 on ZSM-5 using the CLD method, and found that the sorption rate can be enhanced or decreased depending on the structure of the probe molecules and the surface properties of zeolites. Since different batches of the same zeolite can have different properties, one may reach improper conclusions on the nature of surface barriers by simply comparing the effects of surface modification for different zeolite samples. Moreover, the effects of HF etching and SiO_2 deposition have not been studied in the same zeolite sample up to now. Therefore, in this work, the two surface treatments on the same zeolite sample are conducted to probe the nature of surface barriers on zeolites in a self-consistent manner.

ZSM-5 as catalyst or adsorbent is widely used for large-scale applications in the industry. Normal heptane is one important feedstock that can undergo isomerization, cracking, or aromatization in zeolites to produce valuable petrochemicals [40, 41], e.g., propylene and ethylene. Besides, the surface barriers for mass transfer of *n*-heptane in ZSM-5 have not been explored to the best of our knowledge. Hence, it is of both industrial and academic importance to take sorption of *n*-heptane in ZSM-5 as the research system.

In this study, first the presence of significant surface barriers for mass transfer of *n*-heptane in ZSM-5, through comparing the apparent diffusivities of *n*-heptane (measured by the ZLC method) for four ZSM-5 samples with different crystal sizes (1207 – 47 nm), is proven. Then, the ZSM-5 sample with a crystal size of 214 nm is post-treated through HF acid etching and SiO_2 deposition to remove its surface layer and deposit a layer of amorphous SiO_2 on its surface, respectively. Eventually, the effects of HF etching and SiO_2 deposition on the apparent diffusivities are quantified, compared, and analyzed to probe the nature of surface barriers for mass transfer of *n*-heptane in ZSM-5.

2 Experimental

2.1 Synthesis of ZSM-5

Four ZSM-5 samples with different crystal sizes were synthesized by the hydrothermal method. The Si source, Al source, molecular composition of the reaction mixture, and hydrothermal conditions are summarized in Tab. 1.

The synthesis protocol for ZSM-5@1200 and ZSM-5@540 was based on the one reported by Aguado et al. [42] and is briefly described as follows. Appropriate amounts of aluminum isopropoxide (AIP, $Al_2O_3 \geq 24.7$ wt %, Sinopharm Chemical Reagent Co., Ltd.), sodium hydroxide (≥ 96.0 wt %, Sinopharm Chemical Reagent Co., Ltd.), deionized water, and tetrapropylammonium hydroxide (TPAOH , 25 wt % in aqueous solution, Shanghai Macklin Biochemical Co., Ltd.) were mixed and stirred at room temperature until the mixture was clear, forming solution A. Anhydrous ethanol (99.7 wt %, Shanghai Titan Scientific Co., Ltd.) was added to tetraethyl orthosilicate (TEOS, $SiO_2 \geq 28.0$ wt %, Shanghai Lingfeng Chemical Reagent Co., Ltd.), resulting in solution B. Thereafter, solution B was dropwise added into solution A, and the mixture was stirred at room temperature for 12 h to ensure the complete hydrolysis of TEOS. The prepared mother solution was hydrothermally treated in a Teflon-lined, stainless steel autoclave under the hydrothermal conditions given in Tab. 1.

The synthesis protocols for ZSM-5@215 and ZSM-5@50 were both based on the one reported in the literature [43]. The two protocols were similar, except for the use of different Si sources, the former adopting TEOS, the latter employing fumed SiO_2 (Aladdin Industrial Co., Ltd.). The Si source (TEOS or fumed silica) and TPAOH were mixed and stirred at room temperature for 20 h, obtaining solution A. Aluminum trinitrate ($Al(NO_3)_3 \cdot 9H_2O \geq 99.0$ wt %, Xilong Scientific Co., Ltd.), sodium hydroxide, and deionized water were mixed to form solution B. Afterwards, solution B was dropwise added into solution A, and the mixture was stirred at room temperature for 4 h and then hydrothermally treated under the conditions given in Tab. 1. After the hydrothermal reaction, the product was washed with deionized water and centrifuged repeatedly for three times, and then dried at 353 K for 8 h. Finally, the four ZSM-5 samples were obtained after calcination in air at 823 K for 6 h.

2.2 Surface Modification

2.2.1 HF Etching

The as-synthesized sample, ZSM-5@215, was selected to perform HF etching, due to its well-defined external surface and the strong effect of surface barriers on mass transfer, which are shown in Sects. 3.1 and 3.2. The process of HF etching is described elsewhere [34]. Briefly, 1 g of the non-calcined ZSM-5 sample was added into a Teflon container containing a mixture of 0.6 g of HF solution (HF $\geq$ 99.0 wt %, Shanghai Lingfeng Chemical Reagent Co., Ltd.) and 11 mL of acetone ($\geq$ 99.5 wt %, Shanghai Lingfeng Chemical Reagent Co., Ltd.). The zeolite suspension was stirred for 3 min, then immediately diluted with extensive deionized water and filtered using a polypropylene membrane. After that, the product was further washed with about 2 L of deionized water and then dried at 353 K for 8 h. This product was denoted as ZSM-5@HF-1. ZSM-5@HF-2 was obtained by repeating the same procedure a second time. Finally, ZSM-5@HF-1 and ZSM-5@HF-2 were calcined in air at 823 K for 6 h.

2.2.2 SiO_2 Deposition

ZSM-5@215 was also modified by chemical liquid deposition of TEOS, and the process was described elsewhere [44]. Briefly, 2 g of calcined ZSM-5@215 was suspended in a mixture of anhydrous ethanol and TEOS, then the suspension was heated and refluxed for 1 h at 333 K. Thereafter, the suspension was filtered, and then the product was dried at 393 K for 4 h and calcined in air at 823 K for 6 h. This product was labelled as ZSM-5@SiO_2-1. ZSM-5@SiO_2-2 was synthesized by repeating the above procedure a second time.

2.3 Characterization

The crystalline structure was measured by X-ray diffraction (XRD) using a D8 advance A25 diffractometer (Bruker, Germany) equipped with a Cu Kα radiation source. These measurements were carried out in the range $3° < 2\theta < 50°$ at a rate of 12° per min. The zeolite size and morphology were

Table 1. Si and Al sources, molecular compositions of hydrothermal reaction mixtures, and crystallization conditions.

Sample	Si source	Al source	Molecular composition of reaction mixture	Temperature [K]	Duration [d]
ZSM-5@1200	TEOS	AIP	TPAOH/Na_2O/Al/Si/H_2O/EtOH 6.2:1.4:1.0:40.0:236.8:407.0	443	3
ZSM-5@540	TEOS	AIP	TPAOH/Na_2O/Al/Si/H_2O/EtOH 6.2:1.4:1.0:40.0:236.8:407.0	363	3
ZSM-5@215	TEOS	$Al(NO_3)_3$	TPAOH/Na_2O/Al/Si/H_2O 0.1:0.025:1.0:40.0:5.7	443	2
ZSM-5@50	Fumed SiO_2	$Al(NO_3)_3$	TPAOH/Na_2O/Al/Si/H_2O 0.1:0.025:1.0:40.0:5.7	443	1

determined by scanning electron microscopy (SEM) using a NOVA Nano SEM450 microscope (FEI, USA) operating at 3 kV. Transmission electron microscopy (TEM) analysis was conducted on a JEM 2100 instrument (JOEL, Japan) operating at 200 kV. The textural properties of zeolites were determined from N_2 adsorption and desorption measurements at a temperature of 77 K using an ASAP 2020 instrument (Micromeritics, USA).

2.4 Zero Length Column Method

The apparent diffusivities of *n*-heptane in ZSM-5 zeolites at 373, 383, 393, and 403 K were measured by the ZLC method developed by Ruthven et al. [45 – 48]. The temperature should not be too high, as some reactions (i.e., cracking and isomerization) may occur and the corresponding instrumental error cannot be ignored; also the temperature should not be too low as well, as capillary condensation may occur. Prior to the measurements, the sample placed between two stainless steel frits was activated under helium flow at 473 K overnight. After the activation, the sample was initially saturated with *n*-heptane (0.012 vol. %) that was obtained by bubbling helium in a saturator loaded with *n*-heptane and kept at 265 K. Then, the gas flow was switched to pure helium to desorb *n*-heptane, and the transient effluent concentration was measured by a flame ionization detector (FID). The flow rate of 100 mL min^{-1} was selected to carry out the measurements in the kinetically controlled regime, because increasing the flow rate from 80 to 100 mL min^{-1} does not change the long-time slope (see Fig. S1 in the Supporting Information). The isotherm of *n*-heptane was assumed to follow Henry's law [49 – 51] under the experimental conditions in this work, therefore, the apparent diffusivity of *n*-heptane (D_{app}) can be obtained using a long-time analysis, from the desorption curve described by [45, 47]:

$$\frac{c}{c_0} = 2L \sum_{n=1}^{\infty} \frac{\exp\left(-\beta_n^2 \frac{D_{app}}{R^2} t\right)}{\left[\beta_n^2 + L(L-1)\right]} \quad (1)$$

Here, c is the transient effluent concentration of *n*-heptane; c_0 is the initial concentration in the effluent; R is the individual crystal radius of the zeolite sample determined by $(4/3)\pi R^3 = V_{crystal}$ and used in Eq. (4) to calculate the apparent diffusivity; t is the desorption time; the eigenvalues β_n are given by:

$$\beta_n \cot(\beta_n) + L - 1 = 0 \quad (2)$$

and L is:

$$L = \frac{1}{3} \frac{FR^2}{KV_s D_{app}} \quad (3)$$

where F is the interstitial gas velocity, K is Henry's law constant, and V_s is the solid volume in the ZLC cell. In the long-time regime, Eq. (1) can be reduced to

$$\frac{c}{c_0} = \frac{2L}{\beta_1^2 + L(L-1)} \exp\left(-\beta_1^2 \frac{D_{app}}{R^2} t\right) \quad (4)$$

where D_{app}/R^2 can be obtained from the long-time slope when plotting $\ln(c/c_0)$ versus time, t.

3 Results and Discussion

3.1 Characterization of ZSM-5 Samples

3.1.1 Properties of ZSM-5 with Different Crystal Sizes

The structure, morphology, and texture of the four as-synthesized ZSM-5 samples were characterized by XRD, SEM, TEM, and N_2 adsorption. Their main features are summarized in Tab. 2. The XRD patterns of the four ZSM-5 samples are compared in Fig. 1. All patterns show the diffraction peaks for the MFI-type structure and the peak intensities are very high, indicating high crystallinity of the ZSM-5 samples.

Based on SEM images, shown in Fig. 2, ZSM-5@1200, ZSM-5@540, and ZSM-5@215 have a similar shape, but dif-

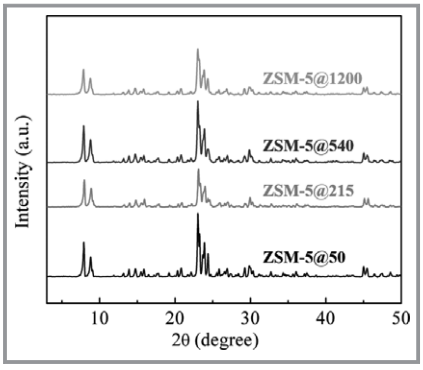

Figure 1. Wide-angle powder XRD patterns of the as-synthesized ZSM-5 samples.

Table 2. Characteristics of the ZSM-5 zeolites with different crystal sizes in this work.

Properties	ZSM-5@1200	ZSM-5@540	ZSM-5@215	ZSM-5@50
Crystal size [nm][a)]	1207	540	214	47
R [nm]	526	229	119	25
S_{BET} [m^{2}g^{-1}]	310	320	357	366
V_{total} [cm^{3}g^{-1}]	0.18	0.19	0.30	0.29
V_{micro} [cm^{3}g^{-1}]	0.12	0.10	0.10	0.12

[a)] Average length of crystal determined from SEM; the crystal is treated as a cuboid for this calculation.

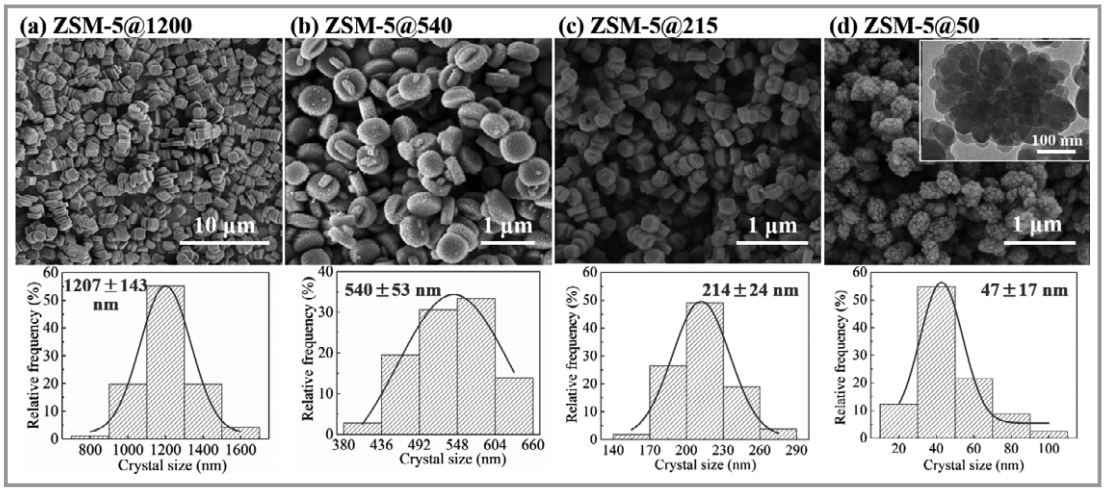

Figure 2. Representative SEM images of a) ZSM-5@1200, b) ZSM-5@540, c) ZSM-5@215, and d) ZSM-5@50. The corresponding histograms of their crystal size distribution are also given below the SEM images. Inserted within a yellow frame in d) is a TEM image of an aggregate of ZSM-5@50 crystals.

ferent surface roughness and crystal size. ZSM-5@1200 and ZSM-5@215 possess relatively smooth surfaces; ZSM-5@540 displays very coarse external surfaces and crystal twinning or secondary crystal growth; some deep holes (meso- and macropores) in ZSM-5@215 are also observed. The average crystal sizes are 1207, 540, and 214 nm for ZSM-5@1200, ZSM-5@540, and ZSM-5@215, respectively, and the histograms of their crystal size distribution are displayed in Fig. 2. ZSM-5@50 consists of aggregates of nano-sized crystals with an average size of 47 nm (determined from TEM images) and probably possesses some mesoporosity between these crystals, as indicated by the TEM image inserted in Fig. 2d.

N_2 adsorption and desorption isotherms in Fig. 3 show the textural properties of the four ZSM-5 samples, and their BET surface area (S_{BET}), external surface area (S_{ext}), total volume (V_{total}, determined from the adsorbed volume at $p/p^0 = 0.99$), and micropore volume (V_{micro}, calculated by the t-plot method) are summarized in Tab. 2. All samples display a fast uptake at very low partial pressure, indicating the presence of much microporosity. ZSM-5@540 shows a small H4 hysteresis loop ($p/p_0 = 0.12 \sim 0.33$) indicative of the existence of very narrow slit pores that contribute to its surface roughness (Fig. 2b). ZSM-5@215 and ZSM-5@50 display a H3 hysteresis loop, suggesting the existence of mesopores in the two samples. For ZSM-5@215, some mesopores lie in the crystals (Fig. 2c); for ZSM-5@50, the mesopores are the voids between the nano-sized crystals (Fig. 2d).

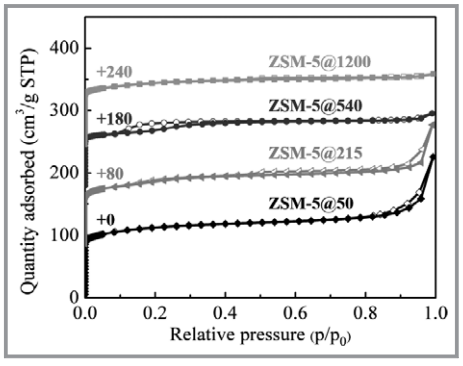

Figure 3. N_2 adsorption (solid symbols) and desorption (open symbols) isotherms at 77 K on the ZSM-5 samples.

3.1.2 Properties of ZSM-5 After Treatment with HF

ZSM-5@215 was post-treated with HF solution once (ZSM-5@HF-1) or twice (ZSM-5@HF-2), for 3 min each time. The SEM images of the parent zeolite and the two post-treated zeolites are shown in Fig. 4. After HF etching once, many more surface voids are formed on ZSM-5@HF-1, implying that some substances were successfully removed from the surface layer. After HF treatment twice, numerous large holes penetrate deeply into the crystals, suggesting that further HF etching is unnecessary to modify the surface structure of the parent sample, as this leads to over-etching of the sample. Valtchev et al. [52] have confirmed that HF solution preferentially removes the amorphous phase on the ZSM-5 crystals. Therefore, the amorphous phase on ZSM-5@215 should be removed after just one HF etching treatment.

3.1.3 Properties of ZSM-5 After Treatment with Tetraethyl Orthosilicate

ZSM-5@215 was post-treated with TEOS once or twice using the CLD method, the TEM images of the parent zeolite and two post-treated zeolites are displayed in Fig. 5. After the first treatment with TEOS, no amorphous SiO_2 is observed in the TEM images, although a very small amount of SiO_2 might have deposited on the zeolite surface; after the second chemical liquid deposition of TEOS, a uniform layer of amorphous SiO_2 with a thickness around 4.4 nm is

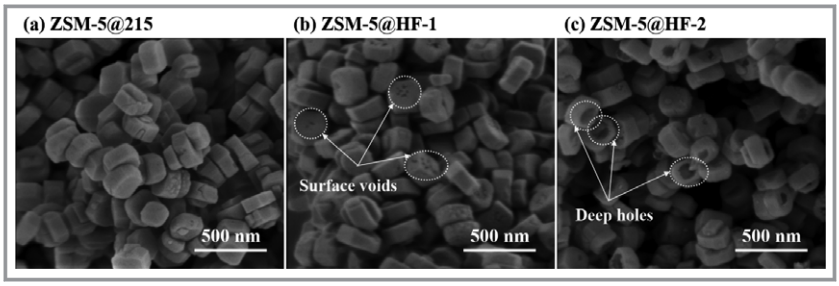

Figure 4. Representative SEM images of a) ZSM-5@215 (parent sample), b) ZSM-5@HF-1 (HF etching for one time), and c) ZSM-5@HF-2 (HF etching for two times).

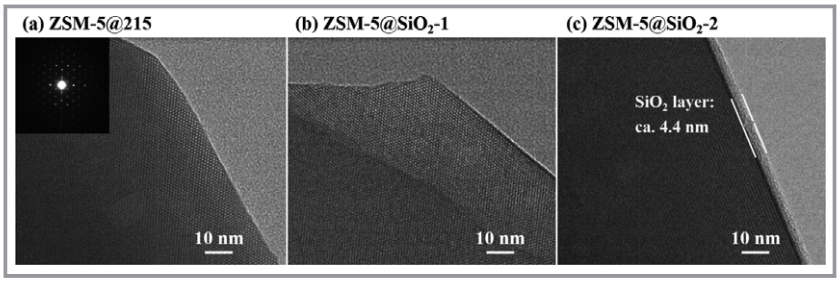

Figure 5. Representative TEM images of a) ZSM-5@215 (parent sample), b) ZSM-5@SiO_2-1 (single SiO_2 deposition step), and c) ZSM-5@ SiO_2-2 (two SiO_2 deposition steps). The insert in a) is the SAED pattern that indicates the single-crystalline nature of ZSM-5@215.

clearly shown in Fig. 5c, indicating the successful deposition of SiO_2 over the surface of ZSM-5@215.

3.2 Strong Surface Barriers for *n*-Heptane Diffusion in ZSM-5

ZLC curves were measured at temperatures of 373, 383, 393, and 403 K for desorption of *n*-heptane from the ZSM-5 samples, as shown in Fig. 6. The apparent diffusivities determined from the ZLC curves are collected in an Arrhenius plot (Fig. 7), and the calculated activation energies are also given. The apparent diffusivity decreases over two orders of magnitude when crystal size decreases from 1207 to 47 nm, which indicates the existence of strong surface barriers. A similar relation between zeolite size and apparent diffusivity was found by Dauenhauer et. al [7, 8, 13] as well as Gobin et al. [9] The activation energies for SM-5@1200, ZSM-5@540, and ZSM-5@215 (26.7, 25.3 and 27.1 kJ mol^{-1}) are very close, while the one (31.7 kJ mol^{-1}) for ZSM-5@50 is 17 – 25 % higher than the other ones.

The apparent diffusivity is expected to be unchanged with zeolite size if the overall mass transport rate is controlled by intracrystalline diffusion. However, when transport across the surface becomes important, the apparent diffusivity would decrease with the reduction of zeolite size, which was regarded as an indirect proof of strong surface barriers [7 – 9, 13]. In this study the same conclusion was made, confirming the presence of strong surface barriers for desorption of *n*-heptane from ZSM-5 crystals. The difference in activation energy can be attributed to the different surface properties of the ZSM-5 samples. ZSM-5@50 has a distinct surface morphology when comparing it to the other ZSM-5 samples (see Fig. 2), and this sample may contain more structural imperfections. Some structural imperfections, such as surface pore narrowing and misalignment, potentially increase the energy barrier for desorption of *n*-heptane from surface pores, and subsequently result in the higher activation energy for ZSM-5@50, as the probe molecules need to overcome this energy barrier [9, 28, 53].

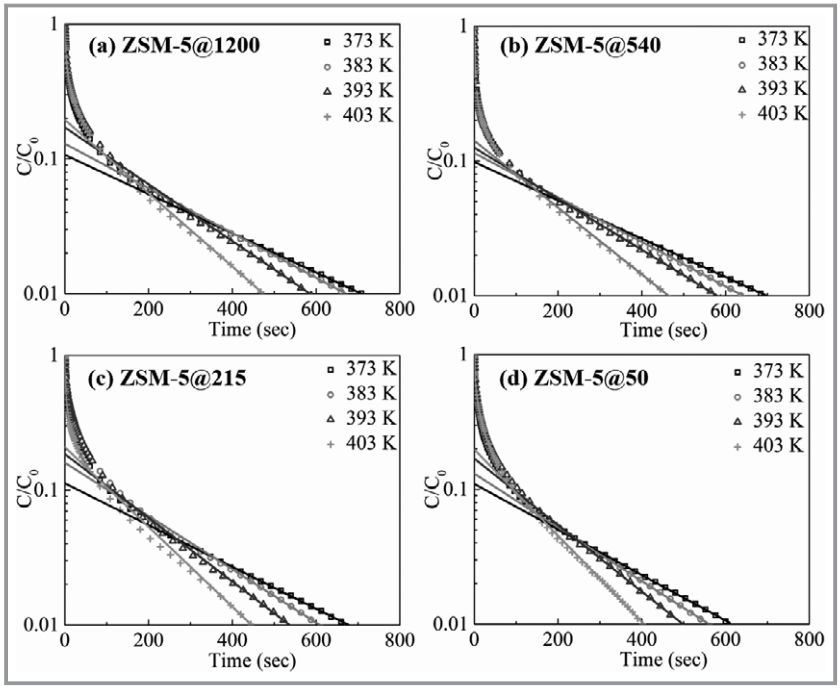

Figure 6. ZLC desorption curves for *n*-heptane in a) ZSM-5@1200, b) ZSM-5@540, c) ZSM-5@215 and d) ZSM-5@50 at 373 K (outlined box), 383 K (outlined circle), 393 K (outlined triangle), and 403 K (cross). Symbols represent experimental data, and solid lines are from the long-time analysis fitting. Flow rate 100 mL min^{-1}, atmospheric pressure.

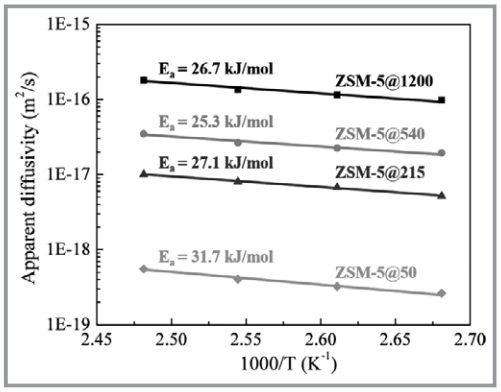

Figure 7. Arrhenius plot for apparent diffusivities of *n*-heptane in ZSM-5@1200 (box), ZSM-5@540 (circle), ZSM-5@215 (triangle), and ZSM-5@50 (diamond). Symbols represent experimental data, and solid lines are the fitted curves. Flow rate 100 mL min^{-1}, atmospheric pressure.

3.3 Effects of HF Etching on Surface Barriers

To probe the effects of HF etching on surface barriers, the apparent diffusivities of *n*-heptane for ZSM-5@215, ZSM-5@HF-1, and ZSM-5@HF-2 are compared in Fig. 8d. The apparent diffusivities for ZSM-5@HF-1 are almost the same as the ones for ZSM-5@215, indicating that HF etching does not affect the surface barriers. The apparent diffusivities for ZSM-5@HF-2 increase by 13 – 31 %, which was anticipated, since the intracrystalline diffusion path is shortened due to the presence of numerous deep holes (see Fig. 4c). In addition, the activation energy for ZSM-5@HF-2 is 18 % higher than the one for ZSM-5@215.

The amorphous phase dissolved by HF solution may fail to block surface pores or change the surface energy barrier in the materials, therefore, the surface barriers are unchanged after HF etching once. However, if the zeolite sample is over-etched by HF solution, some new surface layers are exposed, due to the presence of numerous large holes (see Fig. 4c). These surface layers may be rich in structural imperfections, especially surface pore narrowing and misalignment, which can increase the activation energy [8, 28].

3.4 Effects of SiO_2 Deposition on Surface Barriers

The apparent diffusivities for ZSM-5@215, ZSM-5@SiO_2-1, and ZSM-5@SiO_2-2 are compared in Fig. 9d to study the effects of SiO_2 deposition on surface barriers. The apparent diffusivities for ZSM-5@SiO_2-1 slightly increase by 3 – 12 %, as only very little amorphous SiO_2 is deposited on the zeolite surface after the first treatment with TEOS. However, the apparent diffusivities for ZSM-5@SiO_2-2 are 142 – 187% larger than the ones for ZSM-5@215. In addition, the measured activation energy decreases by 11 to 13 % after SiO_2 deposition once or twice, although there is not enough information from ZLC to conclude that the difference in activation energy between these samples is significant.

The amorphous SiO_2 deposited on ZSM-5 can change the physical nature of the surface layer. Gobin et al. [28] suggested that this physical change could be, in principle: (1) complete pore blockage, (2) surface pore narrowing, or (3) rigidity of the surface pore openings, which essentially increases surface barriers. Thus, this amorphous SiO_2 probably reduces the energy barrier for desorption of *n*-heptane from surface pores, which could be the reason for the decreased activation energy and surface barriers.

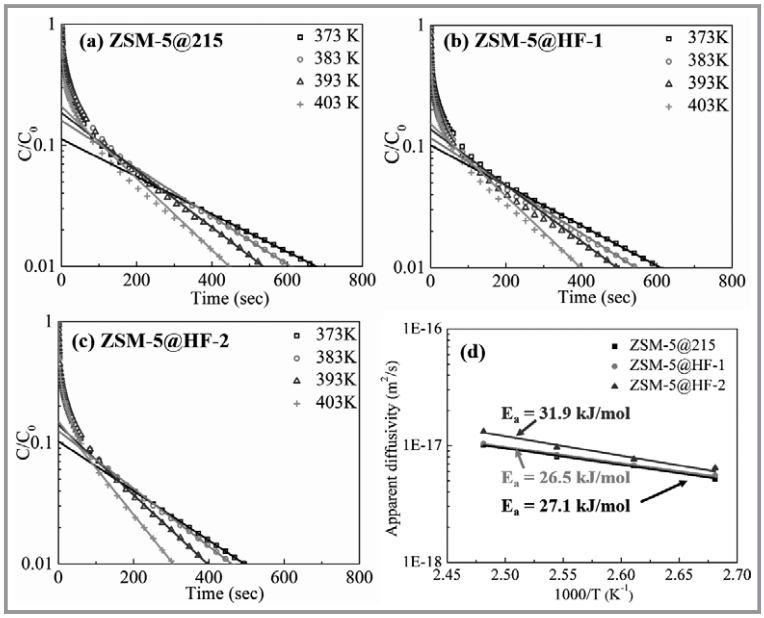

Figure 8. ZLC desorption curves for *n*-heptane in a) ZSM-5@215, b) ZSM-5@HF-1, and c) ZSM-5@HF-2 at 373 K (outlined box), 383 K (outlined circle), 393 K (outlined triangle), and 403 K (cross). d) Arrhenius plot of apparent diffusivities for the three ZSM-5 samples. Symbols represent experimental data, and solid lines are the fitted curves. Flow rate 100 mL min^{-1}, atmospheric pressure.

3.5 The Nature of External Surface Barriers in ZSM-5

The desorption of molecules from zeolite interior to gas phase includes three consecutive steps [11, 12]: (1) diffusing from the interior to a pore mouth, (2) hopping out of a pore mouth and physically adsorbing on the external surface; (3) desorbing into the gas phase. Step 1 is the intracrystalline diffusion, while surface barriers originate from steps 2 and 3. Moreover, desorbing molecules from external surface to gas phase is relatively easy, and the sticking coefficients are generally very low ($10^{-6} \sim 10^{-7}$) [11, 12, 28, 38]. Therefore, hopping out of a pore mouth (step 2) should be the rate determining step of surface

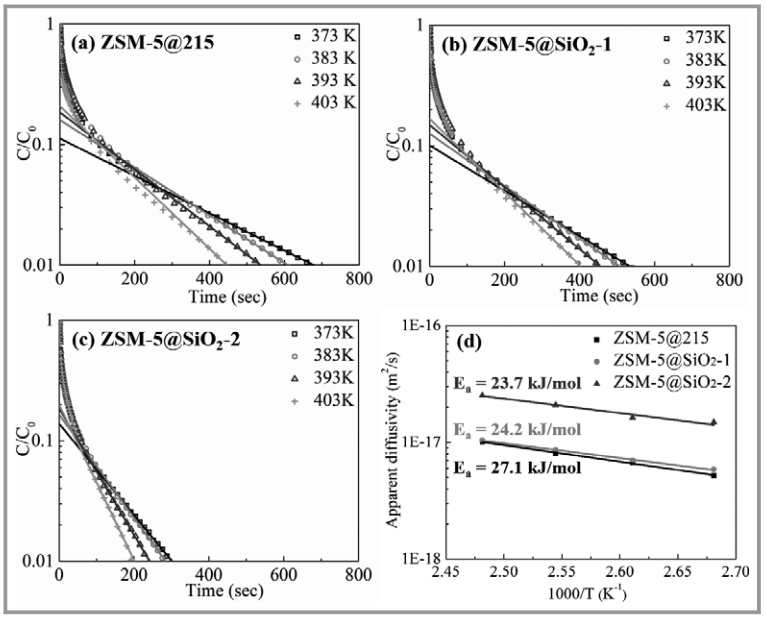

Figure 9. ZLC desorption curves for *n*-heptane in a) ZSM-5@215, b) ZSM-5@SiO_2-1, and c) ZSM-5@SiO_2-2 at 373 K (outlined box), 383 K (outlined circle), 393 K (outlined triangle), and 403 K (cross). d) Arrhenius plot of apparent diffusivities for the three ZSM-5 samples. Symbols represent experimental data, and solid lines are the fitted curves. Flow rate 100 mL min^{-1}, atmospheric pressure.

transport; the surface properties affect this step and, subsequently, the surface barriers.

Surface pore blockage exists when amorphous phase (i.e., SiO_2) covers the external surface of zeolites. This blockage potentially extends the diffusion path length, because additional movements are required before the probe molecule finds an open surface pore, however, the blockage should not change the activation energy [7, 8, 13]. In this work, HF acid was used to dissolve the amorphous phase on ZSM-5@215, and no reduction in surface barriers was found. The external surface of the parent sample is relatively smooth, so it is speculated that there exists only a very small amount of amorphous phase, which is not abundant enough to block many surface pores. Therefore, it is suggested that pore blockage by the amorphous phase should not be the primary reason for surface barriers in the present situation.

An energy barrier exists when a molecule hops out of a pore mouth, because the molecule experiences distinct force fields at the sites on the external surface and in a pore mouth [18, 19, 22]. The molecule needs to overcome this high energy barrier before adsorbing on the external surface, which can cause surface barriers even for zeolites free of structural imperfections. The amorphous SiO_2 near the surface pores can reduce this energy barrier, although it could also narrow or even block the surface pores, according to the work by Lercher et al. [28, 38, 39]. The probe molecule, *n*-heptane, is relatively small compared to the micropore sizes of ZSM-5 and, therefore, the change in energy barrier is more important in affecting surface barriers. In this work, a reduction in surface barriers was found when depositing a layer of amorphous SiO_2 on the external surface of ZSM-5@215, which suggests the energetic nature of surface barriers on zeolites.

It should be noted that structural imperfections can also block the surface pores and contribute to the energy barrier [8, 13, 28, 50]. However, these effects of structural imperfections could not be studied in this work, due to the lack of proper surface modification methods and characterization techniques.

4 Conclusions

In this study, four ZSM-5 samples with different crystal sizes (namely 1207, 540, 214, and 47 nm) were synthesized, and the sample with a crystal size of 214 nm was post-treated through HF acid etching and chemical liquid deposition of TEOS. The apparent diffusivities of *n*-heptane for these ZSM-5 samples were measured, compared, and analyzed to explore the nature of surface barriers. The apparent diffusivity decreases by over two orders of magnitude when reducing the crystal size from 1207 to 47 nm, proving the presence of strong surface barriers in this research system. HF etching cannot change the apparent diffusivity, as long as the sample is not over-etched, thus, suggesting that mechanical pore blockage by amorphous phase should not be the primary reason for surface barriers in this system. SiO_2 deposition increases the apparent diffusivity by over 140 %, as surface barriers are reduced through lowering the energy barrier for desorption of *n*-heptane from surface pores.

Surface barriers possess an energetic or mechanical nature, and the barriers are dependent on the structure of the probe molecules and the surface properties of zeolites. In this work, the large energy barrier should be one important reason for surface barriers; a small amount of amorphous phase cannot affect surface barriers in this case, although it might block or narrow some surface pores. To understand the exact nature of surface barriers under a broader range of conditions, further work on correlating apparent diffusivities with surface properties of zeolites is still needed.

X. G. is supported by the National Natural Science Foundation of China (91434117); G. Y. is supported by the China Postdoctoral Science Foundation (2016M600289) and the Fundamental Research Funds for the Central Universities (222201714004 and 222201718003); M.-O. C is grateful for the financial support by the EPSRC via a "Frontier Engineering" Award (EP/K038656/1).

Symbols used

c	[mol m^{-3}]	transient effluent concentration
c_0	[mol m^{-3}]	initial concentration in the effluent
F	[m s^{-1}]	interstitial gas velocity
K	[Pa m^{3}mol^{-1}]	Henry's law constant
R	[m]	individual crystal radius
S_{BET}	[m^{2}g^{-1}]	BET surface area
S_{ext}	[m^{2}g^{-1}]	external surface area
t	[s]	desorption time
V_{micro}	[cm^{3}g^{-1}]	micropore volume
V_s	[m^3]	solid volume in the ZLC cell
V_{total}	[cm^{3}g^{-1}]	total volume
β_n	[–]	eigenvalues

Abbreviations

AIP	aluminum isopropoxide
CLD	chemical liquid deposition FR frequency response
FID	flame ionization detector
MOF	metal-organic framework
SEM	scanning electron microscopy
TEM	transmission electron microscopy
TEOS	tetraethyl orthosilicate
TPAOH	tetrapropylammonium hydroxide
XRD	X-ray diffraction
ZLC	zero length column

References

[1] B. Smit, T. L. M. Maesen, *Nature* **2008**, *451*, 671 – 678. DOI: 10.1038/nature06552

[2] J. Perez-Ramírez, C. H. Christensen, K. Egeblad, C. H. Christensen, J. C. Groen, *Chem. Soc. Rev.* **2008**, *37 (11)*, 2530 – 2542. DOI: 10.1039/B809030K

[3] W. J. Roth, P. Nachtigall, R. E. Morris, J. Cejka, *Chem. Rev.* **2014**, *114 (9)*, 4807 – 4837. DOI: 10.1021/cr400600f

[4] W. Schwieger, A. G. Machoke, T. Weissenberger, A. Inayat, T. Selvam, M. Klumpp, A. Inayat, *Chem. Soc. Rev.* **2016**, *45 (12)*, 3353 – 3376. DOI: 10.1039/C5CS00599J

[5] R. Chal, C. Gerardin, M. Bulut, S. Van Donk, *ChemCatChem* **2011**, *3 (1)*, 67 – 81. DOI: 10.1002/cctc.201000158

[6] C. C. Chang, A. R. Teixeira, C. Li, P. J. Dauenhauer, W. Fan, *Langmuir* **2013**, *29 (45)*, 13943 – 13950. DOI: 10.1021/la403706r

[7] A. R. Teixeira, C. C. Chang, T. Coogan, R. Kendall, W. Fan, P. J. Dauenhauer, *J. Phys. Chem. C* **2013**, *117 (48)*, 25545 – 25555. DOI: 10.1021/jp4089595

[8] A. R. Teixeira, X. Qi, W. C. Conner, T. J. Mountziaris, W. Fan, P. J. Dauenhauer, *Chem. Mater.* **2015**, *27 (13)*, 4650 – 4660. DOI: 10.1021/acs.chemmater.5b01046

[9] O. C. Gobin, S. J. Reitmeier, A. Jentys, J. A. Lercher, *J. Phys. Chem. C* **2009**, *113 (47)*, 20435 – 20444. DOI: 10.1021/jp907444c

[10] S. M. Rao, E. Saraci, R. Gläser, M.-O. Coppens, *Chem. Eng. J.*, in press. DOI: 10.1016/j.cej.2017.04.015

[11] S. J. Reitmeier, R. R. Mukti, A. Jentys, J. A. Lercher, *J. Phys. Chem. C* **2008**, *112 (7)*, 2538 – 2544. DOI: 10.1021/jp077339t

[12] A. Jentys, H. Tanaka, J. A. Lercher, *J. Phys. Chem. B* **2005**, *109 (6)*, 2254 – 2261. DOI: 10.1021/jp0488362

[13] A. R. Teixeira, X. Qi, C.-C. Chang, W. Fan, W. C. Conner, P. J. Dauenhauer, *J. Phys. Chem. C* **2014**, *118 (38)*, 22166 – 22180. DOI: 10.1021/jp507212b

[14] F. Hibbe, C. Chmelik, L. Heinke, S. Pramanik, J. Li, D. M. Ruthven, D. Tzoulaki, J. Kärger, *J. Am. Chem. Soc.* **2011**, *133 (9)*, 2804 – 2807. DOI: 10.1021/ja108625z

[15] L. Heinke, J. Kärger, *Phys. Rev. Lett.* **2011**, *106 (7)*, 074501. DOI: 10.1103/PhysRevLett.106.074501

[16] P. Kortunov, S. Vasenkov, C. Chmelik, J. Kärger, D. M. Ruthven, J. Wloch, *Chem. Mater.* **2004**, *16 (18)*, 3552 – 3558. DOI: 10.1021/cm0401645

[17] J. R. Agger, N. Hanif, C. S. Cundy, A. P. Wade, S. Dennison, P. A. Rawlinson, M. W. Anderson, *J. Am. Chem. Soc.* **2003**, *125 (3)*, 830 – 839. DOI: 10.1021/ja020899f

[18] N. E. R. Zimmermann, S. P. Balaji, F. J. Keil, *J. Phys. Chem. C* **2012**, *116 (5)*, 3677 – 3683. DOI: 10.1021/jp2112389

[19] N. E. R. Zimmermann, B. Smit, F. J. Keil, *J. Phys. Chem. C* **2012**, *116 (35)*, 18878 – 18883. DOI: 10.1021/jp3059855

[20] N. E. R. Zimmermann, T. J. Zabel, F. J. Keil, *J. Phys. Chem. C* **2013**, *117 (1)*, 7384 – 7390. DOI: 10.1021/jp400152q

[21] N. E. R. Zimmermann, B. Smit, F. J. Keil, *J. Phys. Chem. C* **2010**, *114 (1)*, 300 – 310. DOI: 10.1021/jp904267a

[22] J. Gulín-González, A. Schüring, S. Fritzsche, J. Kärger, S. Vasenkov, *Chem. Phys. Lett.* **2006**, *430 (1 – 3)*, 60 – 66. DOI: 10.1016/j.cplett.2006.07.102

[23] P. Bai, E. Haldoupis, P. J. Dauenhauer, M. Tsapatsis, J. I. Siepmann, *ACS Nano* **2016**, *10 (8)*, 7612 – 7618. DOI: 10.1021/acsnano.6b02856

[24] M. G. Ahunbay, J. R. Elliott, O. Talu, *J. Phys. Chem. B* **2004**, *108 (23)*, 7801 – 7808. DOI: 10.1021/jp040002w

[25] A. Schüring, *J. Phys. Chem. C* **2007**, *111 (30)*, 11285 – 11290. DOI: 10.1021/jp071276x

[26] G. Arya, E. J. Maginn, H. Chang, *J. Phys. Chem. B* **2001**, *105 (14)*, 2725 – 2735. DOI: 10.1021/jp003350g

[27] K. S. Glavatskiy, S. K. Bhatia, *Langmuir* **2016**, *32 (14)*, 3400 – 3411. DOI: 10.1021/acs.langmuir.6b00375

[28] O. C. Gobin, S. J. Reitmeier, A. Jentys, J. A. Lercher, *J. Phys. Chem. C* **2011**, *115 (4)*, 1171 – 1179. DOI: 10.1021/jp106474x

[29] Z. Liu, N. Fujita, K. Miyasaka, L. Han, S. M. Stevens, M. Suga, S. Asahina, B. Slater, C. Xiao, Y. Sakamoto, M. W. Anderson, R. Ryoo, O. Terasaki, *Microscopy* **2013**, *62 (1)*, 109 – 146. DOI: 10.1093/jmicro/dfs098

[30] C. Gonzalez, W. Stracke, Z. Lopez, U. Keller, A. Ricker, R. Reichelt, *Microsc. Microanal.* **2004**, *10 (2)*, 224 – 235. DOI: 10.1017/S1431927604040097

[31] Z. Qin, L. Lakiss, J.-P. Gilson, K. Thomas, J.-M. Goupil, C. Fernandez, V. Valtchev, *Chem. Mater.* **2013**, *25 (14)*, 2759 – 2766. DOI: 10.1021/cm400719z

[32] J. Kärger, R. Valiullin, *Chem. Soc. Rev.* **2013**, *42 (9)*, 4172 – 4197. DOI: 10.1039/C3CS35326E

[33] J. Kärger, T. Binder, C. Chmelik, F. Hibbe, H. Krautscheid, R. Krishna, J. Weitkamp, *Nat. Mater.* **2014**, *13 (4)*, 333 – 343. DOI: 10.1038/nmat3917

[34] J. Wloch, *Microporous Mesoporous Mater.* **2003**, *62 (1 – 2)*, 81 – 86. DOI: 10.1016/S1387-1811(03)00395-0

[35] L. Gueudré, N. Bats, E. Jolimaître, *Microporous Mesoporous Mater.* **2012**, *147 (1)*, 310 – 317. DOI: 10.1016/j.micromeso.2011.06.032

[36] C. Chmelik, A. Varma, L. Heinke, D. B. Shah, J. Kärger, F. Kremer, U. Wilczok, W. Schmidt, *Chem. Mater.* **2007**, *19 (24)*, 6012 – 6019. DOI: 10.1021/cm071632o

[37] L. Gueudré, E. Jolimaître, N. Bats, W. Dong, *Adsorption* **2010**, *16 (1 – 2)*, 17 – 27. DOI: 10.1007/s10450-010-9213-6

[38] S. J. Reitmeier, O. C. Gobin, A. Jentys, J. A. Lercher, *Angew. Chem., Int. Ed.* **2009**, *48 (3)*, 533 – 538. DOI: 10.1002/anie.200803869
[39] S. J. Reitmeier, O. C. Gobin, A. Jentys, J. A. Lercher, *J. Phys. Chem. C* **2009**, *113 (34)*, 15355 – 15363. DOI: 10.1021/jp905307b
[40] N. Rahimi, R. Karimzadeh, *Appl. Catal. A Gen.* **2011**, *398 (1 – 2)*, 1 – 17. DOI: 10.1016/j.apcata.2011.03.009
[41] V. M. Akhmedov, S. H. Al-Khowaiter, *Catal. Rev.* **2007**, *49 (1)*, 33 – 139. DOI: 10.1080/01614940601128427
[42] J. Aguado, D. P. Serrano, J. M. Escola, J. M. Rodríguez, *Microporous Mesoporous Mater.* **2004**, *75 (1 – 2)*, 41 – 49. DOI: 10.1016/j.micromeso.2004.06.027
[43] H. Mochizuki, T. Yokoi, H. Imai, R. Watanabe, S. Namba, J. N. Kondo, T. Tatsumi, *Microporous Mesoporous Mater.* **2011**, *145 (1 – 3)*, 165 – 171. DOI: 10.1016/j.micromeso.2011.05.011
[44] X. Hou, Y. Qiu, X. Zhang, G. Liu, *RSC Adv.* **2016**, *6 (59)*, 54580 – 54588. DOI: 10.1039/C6RA10102J
[45] S. Brandani, D. M. Ruthven, *Adsorption* **1996**, *2 (2)*, 133 – 143. DOI: 10.1007/BF00127043
[46] J. R. Hufton, D. M. Ruthven, *Ind. Eng. Chem. Res.* **1993**, *32 (10)*, 2379 – 2386. DOI: 10.1021/ie00022a022
[47] M. Eic, D. M. Ruthven, *Zeolites* **1988**, *8 (1)*, 40 – 45. DOI: 10.1016/S0144-2449(88)80028-9
[48] E. Mangano, S. Brandani, D. M. Ruthven, *Chem. Ing. Tech.* **2013**, *85 (11)*, 1714 – 1718. DOI: 10.1002/cite.201300083
[49] R. Krishna, D. Paschek, *Sep. Purif. Technol.* **2000**, *21 (1 – 2)*, 111 – 136. DOI: 10.1016/S1383-5866(00)00196-9
[50] S. Calero, B. Smit, R. Krishna, *Phys. Chem. Chem. Phys.* **2001**, *3 (19)*, 4390 – 4398. DOI: 10.1039/b103118j
[51] B. Smit, R. Krishna, *Chem. Eng. Sci.* **2003**, *58 (3 – 6)*, 557 – 568. DOI: 10.1016/S0009-2509(02)00580-8
[52] V. Valtchev, E. Balanzat, V. Mavrodinova, I. Diaz, J. El Fallah, J. M. Goupil, *J. Am. Chem. Soc.* **2011**, *133 (46)*, 18950 – 18956. DOI: 10.1021/ja208140f
[53] M. Schenk, S. Calero, T. L. M. Maesen, T. J. H. Vlugt, L. L. Van Benthem, M. G. Verbeek, B. Schnell, B. Smit, *J. Catal.* **2003**, *214 (1)*, 88 – 99. DOI: 10.1016/S0021-9517(03)00023-X